Sulfosalts with Alkaline Earth Metals. Centrosymmetric vs Acentric Interplay in $Ba_3Sb_{4.66}S_{10}$ and $Ba_{2.62}Pb_{1.38}Sb_4S_{10}$ Based on the Ba/Pb/Sb Ratio. Phases Related to Arsenosulfide Minerals of the Rathite Group and the Novel Polysulfide $Sr_6Sb_6S_{17}$

Kyoung-Shin Choi and Mercouri G. Kanatzidis*

Department of Chemistry and Center for Fundamental Materials Research, Michigan State University, East Lansing, Michigan 48824

Received June 12, 2000

The new compounds, $Sr_6Sb_6S_{17}$, $Ba_{2.62}Pb_{1.38}Sb_4S_{10}$, and $Ba_3Sb_{4.66}S_{10}$ were prepared by the molten polychalcogenide salt method. $Sr_6Sb_6S_{17}$ crystallizes in the orthorhombic space group $P2_12_12_1$ with $a = 8.2871(9)$ Å, $b = 15.352(2)$ Å, $c = 22.873(3)$ Å, and $Z = 4$. This compound presents a new structure type composed of $[Sb_3S_7]^{5-}$ units and trisulfide groups, $(S_3)^{2-}$, held together by Sr^{2+} ions. The $[Sb_3S_7]^{5-}$ fragment is formed from three corner-sharing SbS_3 trigonal pyramids. The trisulfide groups are separated from the $[Sb_3S_7]^{5-}$ unit and embedded between the Sr^{2+} ions. $Ba_3Sb_{4.66}S_{10}$ and $Ba_{2.62}Pb_{1.38}Sb_4S_{10}$ are not isostructural but are closely related to the known mineral sulfosalts of the rathite group. $Ba_3Sb_{4.67}S_{10}$ is monoclinic $P2_1/c$ with $a = 8.955(2)$ Å, $b = 8.225(2)$ Å, $c = 26.756(5)$ Å, $\beta = 100.29(3)°$, and $Z = 4$. $Ba_{2.62}Pb_{1.38}Sb_4S_{10}$ is monoclinic $P2_1$ with $a = 8.8402(2)$ Å, $b = 8.2038(2)$ Å, $c = 26.7623(6)$ Å, $\beta = 99.488(1)°$, and $Z = 4$. The Sb atoms are stabilized in SbS_3 trigonal pyramids that share corners to build ribbonlike slabs, which are stitched by Ba/Pb atoms to form layers perpendicular to the *c*-axis. These materials are semiconductors and show optical band gaps of 2.10, 2.14, and 1.64 eV for $Sr_6Sb_6S_{17}$, $Ba_3Sb_{4.66}S_{10}$, and $Ba_{2.62}Pb_{1.38}Sb_4S_{10}$, respectively. Raman spectroscopic characterization is reported. $Sr_6Sb_6S_{17}$, $Ba_3Sb_{4.66}S_{10}$, and $Ba_{2.62}Pb_{1.38}Sb_4S_{10}$ melt congruently at 729, 770, and 749 °C, respectively.

1. Introduction

For the past several years, we have explored new phases in the broad class of ternary and quaternary chalcoantimonate compounds.[1−4] We discovered unique structure types stabilized mainly by the ability of Sb^{3+} ions to adopt various local environments and due to numerous ways available to combine thio- and selenoantimonate building units with metal centers. The molten flux method has been a superb tool for this type of exploratory synthesis. The flux forms by the in situ fusion of A_2Q (A = alkali metals; Q = chalcogen), Sb/Sb_2Q_3, and chalcogen atoms. Alkali metals from the flux usually incorporate into the structure and occupy cavities in the anionic framework. Recently, we extended the flux approach to alkaline earth metal chalcogenide fluxes. Alkaline earth metals are smaller and possess higher positive charge than alkali metals and, therefore, can lead to different structure types. To date, only a few alkaline earth chalcoantimonates have been reported (e.g. $Ba_4Sb_4Se_{11}$,[5] $BaSb_2S_4$,[6] $Sr_3Sb_4S_9$,[7] ABQ_3 (A = Sr, Ba; B = Sb, Bi; Q = Se,Te)[8]), which suggests that further work in this area could produce interesting new chemistry.

Our investigation using $(Sr,Ba)Sb_xS_y$ fluxes resulted in the discovery of three new thioantimonate compounds, $Sr_6Sb_6S_{17}$, $Ba_3Sb_{4.66}S_{10}$, and $Ba_{2.62}Pb_{1.38}Sb_4S_{10}$. The novelty in $Sr_6Sb_6S_{17}$ lies in the presence of discrete trisulfide $(S_3)^{2-}$ groups, which align in rows to generate a new noncentrosymmetric structure type. $Ba_3Sb_{4.66}S_{10}$ and $Ba_{2.62}Pb_{1.38}Sb_4S_{10}$ are similar in structure but not isomorphous. They are closely related to the known lead arsenosulfide minerals, the rathite group, where rathite-I is $(Pb,Tl)_3As_4(As,Ag)S_{10}$,[9] rathite-Ia is $Pb_{3.5}As_{4.5}S_{10}$,[10] rathite-III is $Pb_3As_5S_{10}$,[10] and dufrenoysite is $Pb_4As_4S_{10}$.[11,12] These compounds share basic structural features with one another, but the difference in composition results in slight modification in atomic positions, which causes each compound to adopt a different space group. For example, rathite-I was reported in the centrosymmetric space group, $P2_1/a$, while dufrenoysite and rathite-Ia were reported in the acentric $P2_1$ and exhibit strong piezoelectricity.[10,11] However, the published structure refinements for some of these mineral sulfosalts are incomplete due to the lack of fine structural tools in the early 1960's, when most of these studies were performed. Among these compounds, $Pb_4As_4S_{10}$ is the only one whose formula preserves charge neutrality. The others probably require an introduction of mixed or partial occupancies in certain sites in order to obtain realistic formulae, which can balance charge.

$Ba_3Sb_{4.66}S_{10}$ and $Ba_{2.62}Pb_{1.38}Sb_4S_{10}$ are analogs of these arsenosulfides with substitution of Pb by Ba atoms partly or entirely. Interestingly, $Pb_2Sb_2S_5$, which would be an antimony analogue of $Pb_4As_4S_{10}$, was reported to adopt a different

(1) (a) Choi, K.-S.; Iordanidis, L.; Chondroudis, K.; Kanatzidis, M. G. *Inorg. Chem.* **1997**, *36*, 3804−3805. (b) Hanko, J. A.; Kanatzidis, M. G. *J. Chem. Soc., Chem. Commun.* **1998**, 725−726.
(2) Chung, D.-Y.; Choi, K.-S.; Iordanidis, L.; Schindler, J. L.; Brazis, P. W.; Kannewurf, C. R.; Chen, B.; Hu, S.; Uher, C.; Kanatzidis, M. G. *Chem. Mater.* **1997**, *9*, 3060−3071.
(3) Choi, K.-S.; Hanko, J. A.; Kanatzidis, M. G. *J. Solid State Chem.* **1999**, 147, 309−319.
(4) Choi, K.-S.; Kanatzidis, M. G. *Chem. Mater.* **1999**, *11*, 2013−2018.
(5) Cordier, G.; Cook, R.; Schäfer, H. *Angew. Chem., Int. Ed. Engl.* **1980**, *19*, 324−325.
(6) Cordier, G.; Schäfer, H. *Z. Naturforsch.* **1979**, *34b*, 1053−1056.
(7) Cordier, G.; Schwidetzky, C.; Schäfer, H. *Rev. Chim. Minéral* **1982**, *19*, 179−186.
(8) Cook, R.; Schäfer, H. *Stud. Inorg. Chem.* **1983**, *3*, 757−760.
(9) Marumo, F.; Nowachi, W. *Z. Kristallogr.* **1965**, *122*, 433−456.
(10) Le Bihan, M.-Th. *Bull. Soc. Fr. Miner. Cristallogr.* **1962**, *LXXXV*, 15−47.
(11) Marumo, F.; Nowachi, W. *Z. Kristallogr.* **1967**, *124*, 409−419.
(12) Ribar, B.; Nicca, Ch.; Nowacki, W. *Z. Kristallogr.* **1969**, *130*, 15−40.

10.1021/ic000632m CCC: $19.00
Published on Web 11/15/2000

structure type.[13] The structures of $Ba_3Sb_{4.66}S_{10}$ and $Ba_{2.62}Pb_{1.38}Sb_4S_{10}$ are closely related to each other, but they exhibit fine alterations in the atomic positions due to the difference in the divalent (Ba^{2+}, Pb^{2+}) to trivalent ion (Sb^{3+}) ratios in their compositions as in the case of the rathite group compounds. This modification again affects the polarity of these compounds and makes $Ba_{2.62}Pb_{1.38}Sb_4S_{10}$ a polar noncentrosymmetric structure. The relationship between $Ba_3Sb_{4.66}S_{10}$ and $Ba_{2.62}Pb_{1.38}Sb_4S_{10}$ is similar to those found among the rathite group of minerals. A complete structural study of $Ba_3Sb_{4.66}S_{10}$ and $Ba_{2.62}Pb_{1.38}Sb_4S_{10}$ could provide us with better understanding of the general features of this class of minerals, such as common trends for disordering or partial occupancy for specific sites. Here we report the synthesis, structures, and physicochemical characterization of $Sr_6Sb_6S_{17}$, $Ba_3Sb_{4.66}S_{10}$, and $Ba_{2.62}Pb_{1.38}Sb_4S_{10}$.

2. Experimental Section

2.1. Synthesis. The following reagents were used as obtained: antimony, 99.999%, −200 mesh, Cerac, Milwaukee, WI; sulfur powder, sublimed, JT Baker Co., Phillipsberg, NJ; lead metal, 99.999%, 200 mesh, Cerac, Milwaukee, WI; strontium metal, 99%, granules < 6 mm, and barium metal, 99%, granules < 6 mm, Aldrich, Milwaukee, WI. The BaS was prepared by a stoichiometric reaction of strontium/barium metal and sulfur in liquid NH_3.

$Sr_6Sb_6S_{17}$. The compound was prepared from a mixture of 0.1402 g (1.6 mmol) of Sr, 0.048 g (0.4 mmol) of Sb, and 0.1539 g (4.8 mmol) of S. The reagents were thoroughly mixed, flame-sealed in an evacuated silica tube, and heated at 800 °C for 5 days. The reaction was then cooled to 200 °C at 2 °C/h. Pure red irregular shaped crystals of $Sr_6Sb_6S_{17}$ were obtained by isolation in degassed dimethylformamide (DMF) and water (yield ~50% based on Sb). The crystals are air- and water-stable.

$Ba_3Sb_{4.66}S_{10}$. The compound was prepared from a mixture of 0.1355 g (0.8 mmol) of BaS, 0.144 g (1.2 mmol) of Sb, and 0.1283 g (4.0 mmol) of S. The reagents were thoroughly mixed, flame-sealed in an evacuated silica tube, and heated at 720 °C for 5 days. The reaction was then cooled to 200 °C at 2 °C/h. Pure red irregular shaped crystals of $Ba_3Sb_{4.66}S_{10}$ were obtained by isolation in degassed DMF and water (yield ~60% based on Sb). The crystals are air- and water-stable.

$Ba_{2.62}Pb_{1.38}Sb_4S_{10}$. The compound was prepared from a mixture of 0.102 g (0.6 mmol) of BaS, 0.124 g (0.6 mmol) of Pb, 0.146 g (1.2 mmol) of Sb, and 0.106 g (3.3 mmol) of S. The reagents were thoroughly mixed, flame-sealed in an evacuated silica tube, and heated at 800 °C for 5 days. The reaction was then cooled to 200 °C at 2 °C/h. Pure silvery-red, needlelike crystals of $Ba_{1.31}Pb_{0.69}Sb_2S_5$ were obtained by isolation in degassed DMF and water (yield > 90% based on Sb).

The compositions of the materials were analyzed with a scanning electron microscope (SEM) using Energy Dispersive Spectroscopy (EDS). The homogeneity of each product was confirmed by comparing their powder X-ray diffraction patterns against ones calculated using X-ray single-crystal data.

2.2. Physical Measurements. Solid-State UV/Vis Spectroscopy. Optical diffuse reflectance measurements were performed at room temperature with a Shimadzu UV-3101 PC double-beam, double-monochromator spectrophotometer operating in the 200−2500 nm region. The instrument is equipped with an integrating sphere and controlled by a personal computer. $BaSO_4$ was used as a 100% reflectance standard for all materials. Samples were prepared by grinding them to a fine powder, spreading them on a compacted surface of the powdered standard material, and preloading them into a sample holder. The reflectance versus wavelength data were used to estimate a material's band gap by converting reflectance to absorption data as described previously.[14]

Single-Crystal UV/Vis Spectroscopy. Optical transmission measurements were made at room temperature on single crystals using a Hitachi U-6000 microscopic FT spectrophotometer with an Olympus BH-2 metallurgical microscope over a range of 380−900 nm.

Differential Thermal Analysis. Differential thermal analysis (DTA) experiments were performed on a computer-controlled Shimadzu DTA-50 thermal analyzer. Typically, a sample (~20 mg) of ground crystalline material was sealed in a silica tube under vacuum. A silica tube of equal mass filled with Al_2O_3 was sealed and placed on the reference side of the detector. The samples were heated to 800 °C at 5 °C/min, isothermed for 10 min followed by cooling at −5 °C/min to 50 °C. Residues of the DTA experiments were examined by X-ray powder diffraction. The stability/reproducibility of the samples was monitored by running multiple heating/cooling cycles.

Raman Spectroscopy. Raman Spectra were recorded on a Holoprobe Raman spectrograph equipped with a CCD camera detector using 633 nm radiation from a HeNe laser for excitation. Laser power at the sample was estimated to be about 1 mW, and the focused laser beam diameter was ca.10 μm. A set of 5 scans was needed to obtain good quality spectra. The accumulation time of each scan was 5 s.

2.3. X-ray Crystallography. $Sr_6Sb_6S_{17}$. A single crystal with dimensions 0.25 × 0.03 · 0.07 mm was mounted on the tip of a glass fiber, and intensity data were collected on a Bruker SMART Platform CCD diffractometer using graphite monochromatized Mo Kα radiation. The data were collected at room temperature over a full sphere of reciprocal space, up to 28.71° in θ. The individual frames were measured with an ω rotation of 0.3° and an acquisition time of 45 s. The SMART[15] software was used for the data acquisition and SAINT[16] for the data extraction and reduction. The absorption correction was performed using SADABS.[17] Structure solution and refinement were performed with the SHELXTL package of crystallographic programs.[18] The structure of $Sr_6Sb_6S_{17}$ was solved and refined successfully in the chiral space group, $P2_12_12_1$, which was uniquely defined by the systematic absence conditions of the data set.

$Ba_3Sb_{4.67}S_{10}$. A single crystal with dimensions 0.27 × 0.17 × 0.06 mm was mounted on the tip of a glass fiber, and intensity data were collected on a Bruker SMART Platform CCD diffractometer using graphite monochromatized Mo Kα radiation. The data were collected at room temperature over a full sphere of reciprocal space, up to 28.25° in q. The individual frames were measured with an ω rotation of 0.3° and an acquisition time of 40 s. The data were processed as described above. The structure of $Ba_3Sb_{4.67}S_{10}$ was solved and refined in the centrosymmetric $P2_1/c$ space group. After successive refinement, one of the Sb atoms, Sb(5), showed an abnormally high atomic displacement parameter (ADP), implying a partial occupancy for the site. The occupancy of Sb(5) was refined to be 66.7(3)% without constraints, and this gives a nominal composition of $Ba_3Sb_{4.67}S_{10}$, which satisfies charge neutrality. However, the ADP for Sb(5) remained high, and at this stage we suspected that the Sb atom might be modeled as positionally disordered over more than one site. Unlike other three-coordinate Sb atoms in the structure, Sb(5) occupies a large six-coordinate site and may find more than one proper position to sit in this large pocket. A notable electron density peak was found near the Sb(5) site (0.6 Å apart) and assigned as Sb(5'). Introduction of the positional disorder dropped the ADPs to normal values and the final occupancies for Sb(5) and Sb(5') are 59.5(3) and 7.2(3)%, respectively.

$Ba_{2.62}Pb_{1.38}Sb_4S_{10}$. A single crystal with dimensions 0.31 × 0.10 × 0.04 mm was mounted on the tip of a glass fiber, and intensity data were collected on a Bruker SMART Platform CCD diffractometer using graphite monochromatized Mo Kα radiation. The data were collected at room temperature over a full sphere of reciprocal space, up to 29.00° in θ. The individual frames were measured with an ω rotation of 0.3° and an acquisition time of 60 s. The data were processed as explained

(13) Smith, P. P. K.; Hyde, B. G. *Acta Crystallogr.* **1983**, *C39*, 1498−1502.

(14) McCarthy, T. J.; Ngeyi, S.-P.; Liao, J.-H.; Degroot, D.; Hogan, T.; Kannewurf, C. R.; Kanatzidis, M. G. *Chem. Mater.* **1993**, *5*, 331.

(15) *SMART*; Siemens Analytical Xray Systems, Inc.: Madison, WI, 1994.

(16) *SAINT*, Version 4; Siemens Analytical Xray Systems, Inc.: Madison, WI, 1994−1996.

(17) Sheldrick, G. M. University of Göttingen: Göttingen, Germany, to be published.

(18) Sheldrick, G. M. *SHELXTL*, Version 5; Siemens Analytical X-ray Systems, Inc.: Madison, WI, 1994.

Table 1. Summary of Crystallographic Data and Structural Analysis for $Sr_6Sb_6S_{17}$, $Ba_{2.62}Pb_{1.38}Sb_4S_{10}$, and $Ba_3Sb_{4.66}S_{10}$

formula	$Sr_6Sb_6S_{17}$	$Ba_2(Ba_1,Sb_{0.66})Sb_4S_{10}$	$Ba_2(Pb_{1.38},Ba_{0.62})Sb_4S_{10}$
fw	1801.24	1301.19	1453.88
cryst habit	red, irregular shape	red, irregular shape	silver needle
cryst dimens			
space group	$P2_12_12_1$	$P2_1/c$	$P2_1$
a, Å	8.2871(9)	8.955(2)	8.8402(2)
b, Å	15.352(2)	8.225(2)	8.2038(2)
c, Å	22.873(3)	26.756(5)	26.7623(6)
β, deg	N. A.	100.29(3)	99.488(1)
Z; *V*, Å^3	4; 2909.9(5)	4; 1939.0(7)	4; 1914.34(8)
D_{calc}, g/cm^3	4.112	4.457	5.045
temp, K	298(2)	170(1)	298(2)
λ(Mo Kα), Å	0.71073	0.71073	0.71073
μ(Mo Kα), cm^{-1}	175.90	134.47	240.60
θ_{max}, deg	28.71	28.25	29.00
R indices [$I > 2\sigma$]	R1[a] = 0.0321	R1 = 0.0262	R1 = 0.0579
	wR2[b] = 0.0645	wR2 = 0.0602	wR2 = 0.1509
R indices (all data)	R1 = 0.0446	R1 = 0.0294	R1 = 0.0740
	wR2 = 0.0677	wR2 = 0.0613	wR2 = 0.1586
GOF on F^2	0.978	1.106	0.017
BASF	N.A.	N.A.	0.501(12)

[a] $R1 = \sum||F_o| - |F_c||/\sum|F_o|$. [b] $wR2 = \{\sum[w(F_o^2 - F_c^2)^2]/\sum[w(F_o^2)^2]\}^{1/2}$.

above. The structure of $Ba_{2.62}Pb_{1.38}Sb_4S_{10}$ was solved and refined successfully in the polar and chiral $P2_1$ space group. The crystal used for the structure solution was racemically twinned, and the BASF parameter was refined. After successive refinement, all the Pb sites showed high ADPs, and mixed occupancy with Ba was introduced to these sites. The S(1) and S(5) sites also showed unusually high ADPs, which could not be dropped by refining the occupancies. Near both sites, prominent electron density peaks were found and assigned as S(1') and S(5'), respectively. The sum of the occupancies of S(1) and S(1') was constrained to be the maximum allowed in these crystallographic sites and so was that of the occupancies of S(5) and S(5'). The introduction of positional disorder decreased ADPs to reasonable values.

An attempt to solve the structure in the centrosymmetric space group $P2_1/m$ was made, but it failed because the structure obviously does not possess mirror planes perpendicular to the *b*-axis; see description below. Solving the structure in the centrosymmetric space group, $P2_1/c$ was also considered because its analogue, $Ba_3Sb_{4.67}S_{10}$, adopts the same space group. However, the systematic absence conditions showed that the *c*-glide plane does not exist in this structure (22% of the *h*0*l* reflections with $l = 2n + 1$ are observed with the intensities greater than 3σ). Nevertheless, we still attempted to solve and refine the structure in $P2_1/c$. This gave a significantly higher values of R1 = 14.05 and wR2 = 29.86 for all data.

The complete data collection parameters and details of the structure solution and refinement for each compound are given in Table 1. The coordinates of all atoms, isotropic temperature factors, and their estimated standard deviations (esd's) for each compound are given in Tables 2−4. The selected bond distances for each compound are given in Tables 5−7.

3. Results and Discussion

3.1. Structure. $Sr_6Sb_6S_{17}$. The overall structure of this compound, viewed down the *b*-axis, is shown in Figure 1. It is composed of Sr^{2+} ions stabilized between $[Sb_3S_7]^{5-}$ units and trisulfide groups, $(S_3)^{2-}$. Therefore, the formula can be written as $(Sr^{2+})_6[(Sb_3S_7)^{5-}]_2(S_3^{2-})$, and the compound is formally a polysulfide. There are six independent Sb atoms, all of which are stabilized in trigonal pyramidal sites. The Sb(1), Sb(2), and Sb(3) pyramids are joined together by sharing corners to form $(Sb_3S_7)^{5-}$ units and so are the pyramids Sb(4), Sb(5), and Sb(6); see the inset of Figure 1. This unit has a finite length and does not form an infinite chain. The closest distance between the Sb atom in one unit and sulfur atoms in the neighboring units ranges from 2.981 to 3.436 Å, which are much longer than the average Sb−S bond distance of 2.500 Å in the $(Sb_3S_7)^{5-}$ unit. Nevertheless, if we take this weak Sb−S interaction into consideration, these units appear to form one-dimensional ribbonlike slabs parallel to the *a*-axis; see Figure 2a. Two such slabs are paired by van der Waals interactions to form sandwichlike blocks parallel to the *a*-axis. Between these blocks Sr^{2+} ions are stabilized either in tri- or in monocapped trigonal prismatic sites.

A novel feature of this compound is the presence of discrete trisulfide groups, $(S_3)^{2-}$, which are embedded between these Sr^{2+} ions. The trisulfide group is bent with the S−S−S bond

Table 2. Fractional Atomic Coordinates and Equivalent Isotropic Displacement Parameter Values for $Sr_6Sb_6S_{17}$ with Estimated Standard Deviations in Parentheses

atom	x	y	z	U(eq),[a] Å^2
Sb(1)	0.0002(1)	0.3071(1)	0.2496(1)	0.015(1)
Sb(2)	0.4760(1)	0.2911(1)	0.2318(1)	0.018(1)
Sb(3)	0.5113(1)	0.1814(1)	0.0852(1)	0.017(1)
Sb(4)	0.0087(1)	0.6747(1)	0.4399(1)	0.019(1)
Sb(5)	0.5330(1)	0.4224(1)	0.0917(1)	0.019(1)
Sb(6)	0.0164(1)	0.4281(1)	0.1077(1)	0.018(1)
Sr(1)	0.2444(1)	0.1655(1)	0.3764(1)	0.012(1)
Sr(2)	0.2489(1)	0.6665(1)	0.1247(1)	0.013(1)
Sr(3)	0.2501(1)	0.0498(1)	0.2126(1)	0.017(1)
Sr(4)	0.2462(1)	0.5547(1)	0.2890(1)	0.020(1)
Sr(5)	0.2498(1)	0.0596(1)	0.5449(1)	0.013(1)
Sr(6)	0.2433(1)	0.4429(1)	0.4566(1)	0.014(1)
S(1)	0.2916(3)	0.1467(2)	0.6834(1)	0.019(1)
S(2)	0.2502(3)	0.3448(2)	0.3067(1)	0.016(1)
S(3)	0.0011(3)	0.1540(1)	0.2793(1)	0.013(1)
S(4)	0.5001(3)	0.1503(1)	0.2810(1)	0.014(1)
S(5)	0.2861(3)	0.2316(2)	0.1567(1)	0.015(1)
S(6)	0.5016(3)	0.0294(1)	0.1192(1)	0.014(1)
S(7)	0.7285(3)	0.2288(2)	0.1489(1)	0.017(1)
S(8)	0.2763(3)	0.3723(2)	0.0048(1)	0.018(1)
S(9)	0.0036(3)	0.0384(1)	0.1169(1)	0.014(1)
S(10)	0.7218(3)	0.3761(2)	0.0101(1)	0.016(1)
S(11)	0.4930(3)	0.0680(1)	0.4460(1)	0.012(1)
S(12)	0.2676(3)	0.0272(2)	0.8363(1)	0.016(1)
S(13)	0.0081(3)	0.5623(1)	0.0511(1)	0.014(1)
S(14)	0.2381(3)	0.4765(2)	0.1698(1)	0.021(1)
S(15)	0.4991(3)	0.2959(1)	0.4285(1)	0.014(1)
S(16)	0.1398(2)	0.2488(1)	0.5019(1)	0.012(1)
S(17)	0.0048(3)	0.2938(1)	0.4309(1)	0.013(1)

[a] U(eq) is defined as one-third of the trace of the orthogonalized $\mathbf{U}_{ij}$ tensor.

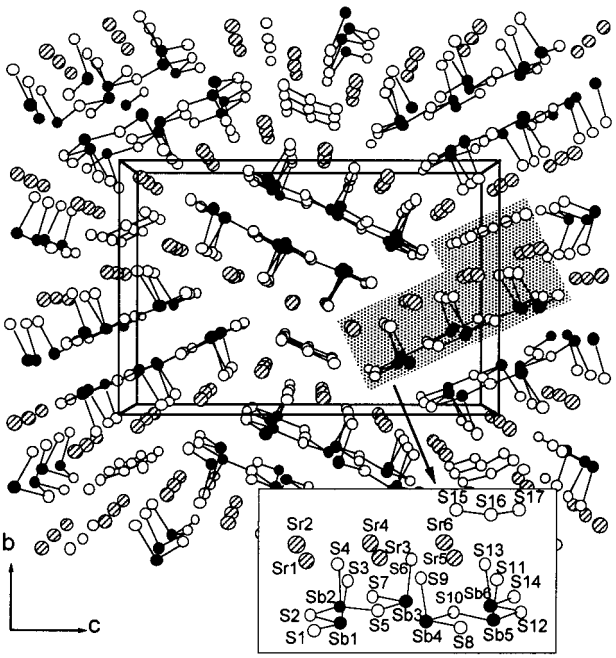

Figure 1. Structure of $Sr_6Sb_6S_{17}$ viewed down the *b*-axis. The inset shows an asymmetric unit with the atomic labeling scheme.

Table 3. Fractional Atomic Coordinates and Equivalent Isotropic Displacement Parameter Values for $Ba_3Sb_{4.66}S_{10}$ with Estimated Standard Deviations in Parentheses

atom	x	y	z	*U*(eq), Å^2
Ba(1)	0.0910(1)	0.6183(1)	0.4317(1)	0.008(1)
Ba(2)	0.5276(1)	0.2686(1)	0.2992(1)	0.007(1)
Ba(3)	0.0233(1)	0.2673(1)	0.2974(1)	0.007(1)
Sb(1)	0.7044(1)	0.3346(1)	0.1606(1)	0.007(1)
Sb(2)	0.2420(1)	0.3132(1)	0.1515(1)	0.009(1)
Sb(3)	0.1421(1)	0.6501(1)	0.0590(1)	0.009(1)
Sb(4)	0.3262(1)	0.1549(1)	0.4554(1)	0.015(1)
Sb(5)[a]	0.4256(1)	0.0357(1)	0.0566(1)	0.019(1)
Sb(5)	0.4183(8)	0.0521(10)	0.0770(5)	0.019(1)
S(1)	0.0813(2)	0.6560(2)	0.3164(1)	0.009(1)
S(2)	0.4928(2)	0.1607(2)	0.1801(1)	0.010(1)
S(3)	0.7403(1)	0.4980(2)	0.2366(1)	0.009(1)
S(4)	0.2471(1)	0.4718(2)	0.2265(1)	0.008(1)
S(5)	0.3754(1)	0.5049(2)	0.1023(1)	0.009(1)
S(6)	0.0424(2)	0.0061(2)	0.4005(1)	0.011(1)
S(7)	0.1777(2)	0.6192(2)	0.6162(1)	0.010(1)
S(8)	0.3144(2)	0.3493(2)	0.3870(1)	0.010(1)
S(9)	0.1736(2)	0.1850(2)	0.0058(1)	0.011(1)
S(10)	0.5833(2)	0.2066(2)	0.0050(1)	0.015(1)

[a] Sb5 and Sb5′ are positionally disordered with occupancy of 59.5(3) and 7.2(3)%, respectively.

angle of 113.75° and the S−S distances of 2.090(3) Å. These values are similar to those observed in BaS_3, Cs_2S_3, Rb_2S_3, and K_2S_3.[19−21] The arrangement of trisulfide groups are shown in Figure 2b. These arrow-shaped anions are well aligned in one direction, forming a polar row. The polarity, however, is canceled by a neighboring row, which runs in the opposite direction making the compound nonpolar, albeit it remains noncentrosymmetric.

$Ba_3Sb_{4.66}S_{10}$ and $Ba_{2.62}Pb_{1.38}Sb_4S_{10}$. Interestingly, these two compounds represent a centrosymmetric and a polar version of the same structural type. The $Ba_3Sb_{4.66}S_{10}$ is composed of Ba^{2+} ions stabilized between two-dimensional layers oriented perpendicular to the *c*-axis. The overall structure of $Ba_3Sb_{4.66}S_{10}$ viewed down the *a*-axis is shown in Figure 3a. Each layer is built from a one-dimensional slab parallel to the *a*-axis stitched together by Ba(1) and Sb(5/5′) ions. Propagation of a single

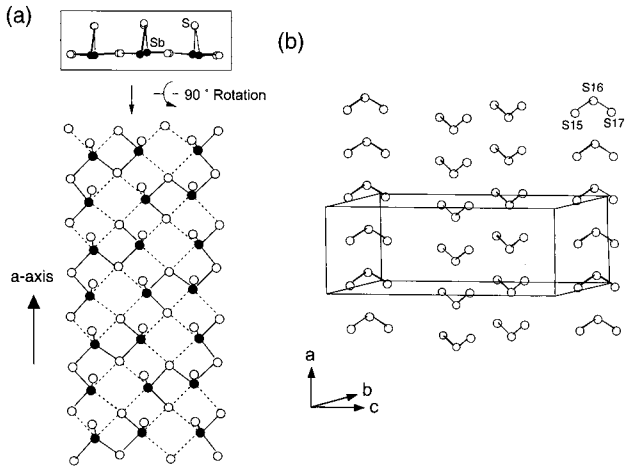

Figure 2. (a) Propagation of a single slab along the *a*-axis The dashed lines represent weak Sb−S interactions between $(Sb_3S_7)^{5-}$ units. (b) Spatial arrangement of the trisulfide groups in $Sr_6Sb_6S_{17}$.

Table 4. Fractional Atomic Coordinates and Equivalent Isotropic Displacement Parameter Values for $Ba_{2.62}Pb_{1.38}Sb_4S_{10}$ with Estimated Standard Deviations in Parentheses

atom	x	y	z	*U*(eq), Å^2
Pb(1)/Ba(1)[a]	0.4124(1)	0.3005(2)	0.8241(1)	0.034(1)
Pb(2)/Ba(2)[b]	0.0947(2)	0.8216(2)	0.1868(1)	0.033(1)
Pb(3)/Ba(3)[c]	0.5994(1)	0.4078(2)	0.6814(1)	0.039(1)
Pb(4)/Ba(4)[d]	0.0815(1)	0.4091(2)	0.6805(1)	0.039(1)
Ba(5)	0.5220(2)	0.1100(2)	0.0451(1)	0.028(1)
Ba(6)	0.0228(2)	0.1022(2)	0.0475(1)	0.031(1)
Ba(7)	0.5224(2)	0.1097(2)	0.5472(1)	0.025(1)
Ba(8)	0.0256(2)	0.1092(2)	0.5470(1)	0.025(1)
Sb(1)	0.2836(2)	0.5513(3)	0.0960(1)	0.036(1)
Sb(2)	0.1840(2)	0.0523(3)	0.9030(1)	0.036(1)
Sb(3)	0.8305(2)	0.2302(3)	0.1999(1)	0.035(1)
Sb(4)	0.3707(2)	0.2297(3)	0.2013(1)	0.036(1)
Sb(5)	0.1427(2)	0.4973(3)	0.2912(1)	0.043(1)
Sb(6)	0.6541(2)	0.4893(2)	0.3068(1)	0.023(1)
Sb(7)	0.6939(3)	0.1630(3)	0.3985(1)	0.053(1)
Sb(8)	0.2042(2)	0.1739(2)	0.4097(1)	0.020(1)
S(1)[e]	0.4950(40)	0.7260(40)	0.0709(12)	0.053(5)
S(1)	0.5690(40)	0.7260(30)	0.0686(11)	0.053(5)
S(2)	0.0413(9)	0.7146(9)	0.0663(3)	0.040(2)
S(3)	0.2574(7)	0.3887(11)	0.0192(3)	0.036(2)
S(4)	0.7620(7)	0.3910(11)	0.0202(3)	0.037(2)
S(5)[f]	0.0298(13)	0.3629(15)	0.1474(5)	0.042(2)
S(5)	0.1240(20)	0.3650(20)	0.1484(8)	0.042(2)
S(6)	0.5766(12)	0.3786(10)	0.1494(3)	0.064(3)
S(7)	0.8073(8)	0.0019(11)	0.1373(3)	0.035(2)
S(8)	0.3355(7)	0.0055(10)	0.1371(3)	0.031(2)
S(9)	0.6230(12)	0.633(12)	0.2543(3)	0.063(3)
S(10)	0.1307(11)	0.672(12)	0.2538(4)	0.062(3)
S(11)	0.3372(6)	0.6519(8)	0.2464(2)	0.024(1)
S(12)	0.0911(6)	0.1559(8)	0.7542(2)	0.024(1)
S(13)	0.1845(7)	0.6931(8)	0.3640(3)	0.025(1)
S(14)	0.3144(7)	0.2273(9)	0.6372(3)	0.030(2)
S(15)	0.4751(5)	0.3517(7)	0.3532(2)	0.019(1)
S(16)	0.8797(5)	0.3510(6)	0.3530(2)	0.017(1)
S(17)	0.7369(6)	0.3136(7)	0.4751(2)	0.019(1)
S(18)	0.2425(7)	0.3380(7)	0.4856(2)	0.022(1)
S(19)	0.4286(6)	0.0004(7)	0.4308(2)	0.018(1)
S(20)	0.0038(5)	0.0000(6)	0.4310(2)	0.013(1)

[a] 72(1)% Pb(1)/28(1)% Ba(1). [b] 36(1)% Pb(2)/63(1)% Ba(2). [c] 83(1)% Pb(3)/17(1)% Ba(3). [d] 87(1)% Pb(4)/13(1)% Ba(4). [e] 49(3)% S(1)/51(3)% S(1′). [f] 63(1)% S(5)/37(1)% S(5′).

(19) (a) Yamaoka, S.; Lemley, J. T.; Jenks, J. M.; Steinfink, H. *Inorg. Chem.* **1975**, *14*, 129−131. (b) Miller, W. S.; King, A. T. *Z. Kristallogr. Kristallgeom. Kristallphys. Kristallchem.* **1977**, *144*, 439−446.
(20) Böttcher, P. *Z. Anorg. Allg. Chem.* **1980**, *461*, 13−21.
(21) Böttcher, P. *Z. Anorg. Allg. Chem.* **1977**, *432*, 167−172.

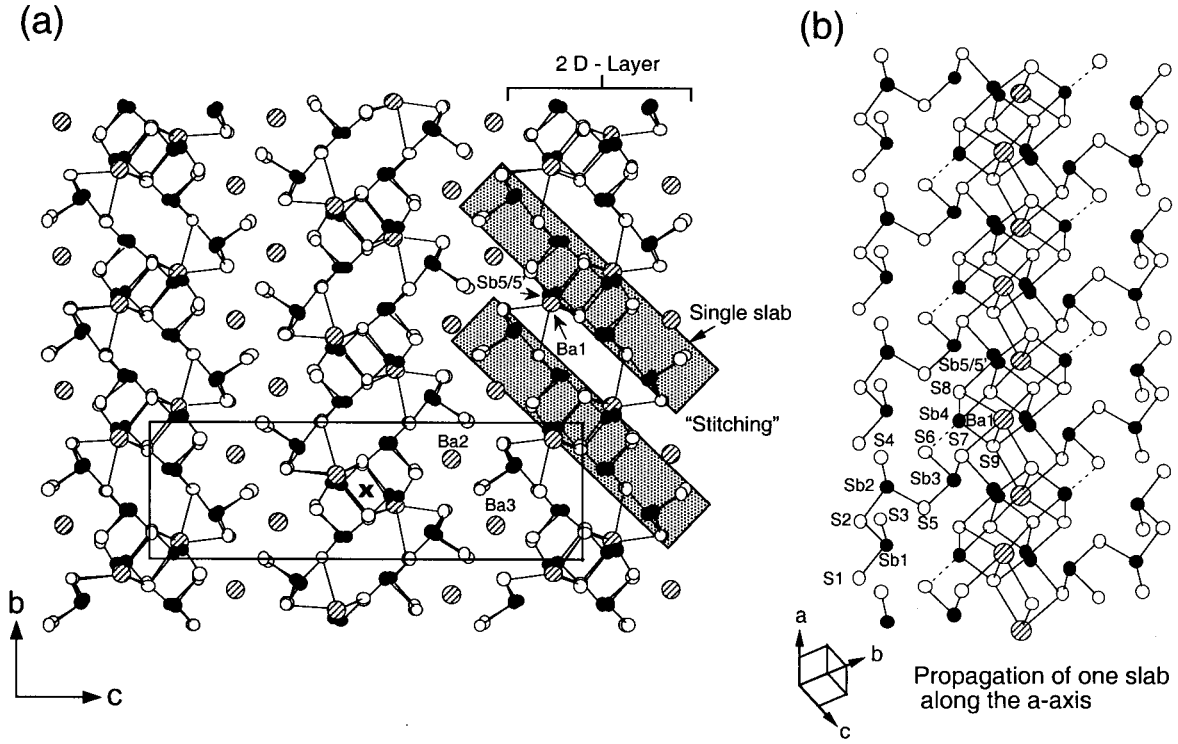

Figure 3. (a) Structure of $Ba_3Sb_{4.66}S_{10}$ viewed down the *a*-axis. (b) Propagation of a single slab along the *a*-axis.

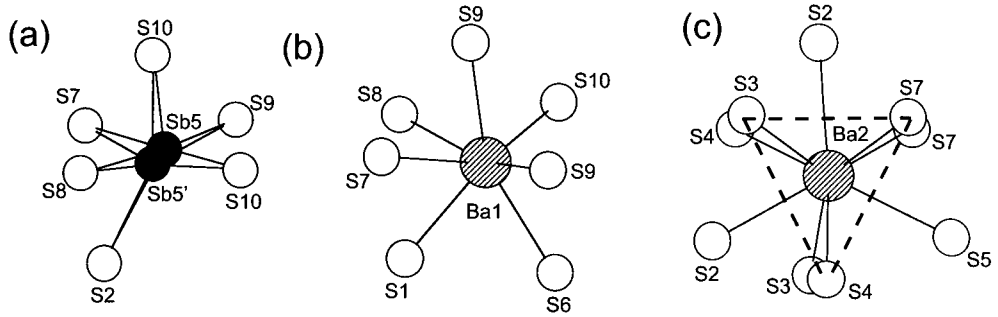

Figure 4. Local environment of Sb(5/5′), Ba(1), and Ba(2) atoms in $Ba_3Sb_{4.66}S_{10}$.

slab along the *a*-axis is shown in Figure 3b with the atomic labeling scheme. There exist five independent Sb atoms in the structure. Sb(1), Sb(2), and Sb(3) are stabilized in three-coordinate trigonal pyramidal sites. These pyramids share corners with one another to from $(Sb_3S_7)^{5-}$ units, as seen in $Sr_6Sb_6S_{17}$. Sb(4) forms its own pyramid, which is weakly attached to the $(Sb_3S_7)^{5-}$ unit since Sb(4) has a moderate interaction with the fourth nearest sulfur atom, S(6) from the $(Sb_3S_7)^{5-}$ unit (2.963(2) Å). The inclusion of Sb(4) results in $(Sb_4S_{11})^{10-}$ fragments, which are connected together by high-coordinate Sb(5/5′) and Ba(1) atoms to form a one-dimensional slab along the *a*-axis. The Sb(5/5′) and Ba(1) atoms are stabilized in basically the same local environment; see Figure 4. The difference is that the seventh nearest sulfur atom from Sb(5/5′) is too far away to be considered bonding (~3.9 Å). The Sb(5/5′) atom is shifted relative to Ba(1) in order to bind more tightly to six sulfur atoms. For the smaller Sb atom, even a six-coordinate site is too spacious, causing the Sb to be positionally disordered over two sites, Sb(5) and Sb(5′). The Sb(5/5′), and Ba(1) atoms play an important role in forming the structure because they serve as stitching points for the $(Sb_4S_{11})^{10-}$ units to build a single slab; see Figure 3. Between these layers, Ba(2) and Ba(3) atoms are stabilized in nine-coordinate tricapped trigonal prismatic sites; see Figure 4.

$Ba_{2.62}Pb_{1.38}Sb_4S_{10}$ is structurally related to $Ba_3Sb_{4.66}S_{10}$; see Figure 5. They can be described as $(Ba_2)(Ba_{0.62},Pb_{1.38})[Sb_4S_{10}]$ and $(Ba_2)(Ba_1,Sb_{0.67})[Sb_4S_{10}]$, respectively, when the cations are separated into three groups depending on their local environment; the first group of cations is nine-coordinate, the second (6 + 1)-coordinate, and the third three-coordinate. This classification clearly shows how $Ba_{2.62}Pb_{1.38}Sb_4S_{10}$ is related to $Ba_3Sb_{4.66}S_{10}$ compositionally. The nine-coordinate Ba sites and three-coodinate Sb sites remain intact in both compounds. It is the (6 + 1)-coordinate sites that can accommodate mixed or partial occupancies and generate a difference in composition. In $Ba_{2.62}Pb_{1.38}Sb_4S_{10}$, the Pb atoms are segregated in the (6 + 1)-coordinate sites, and all are disordered with Ba atoms in different proportions; see Table 4. The coordination environments of the Pb atoms are similar to those of Sb(5) in $Ba_3Sb_{4.66}S_{10}$. These sites are now fully occupied by divalent Pb^{2+}/Ba^{2+} ions, while the Sb(5/5') site in $Ba_3Sb_{4.66}S_{10}$ is only 0.667 occupied by the trivalent Sb^{3+} ions so as to balance the charge. The cationic arrangement pattern of the compound is easily understood by considering the size of cations. The larger Ba^{2+} ions prefer the nine-coordinate sites first, and then the remaining ones are placed along with Pb atoms in the next larger (6 + 1)-coordinate sites. The disorder between Pb and Ba seems to be responsible for the generally high ADPs of the sulfur atoms

Table 5. Selected Distances (Å) for $Sr_6Sb_6S_{17}$

Sb(1)−S(1)	2.417(2)	Sb(2)−S(4)	2.4460(16)
Sb(1)−S(3)	2.4458(16)	Sb(2)−S(5)	2.502(2)
Sb(1)−S(2)	2.517(2)	Sb(2)−S(2)	2.668(2)
Sb(1)−S(5)	3.387(2)	Sb(2)−S(7)	2.981(2)
Sb(1)−S(7)	3.436(3)	Sb(2)−S(1)	3.394(3)
Sb(3)−S(7)	2.428(2)	Sb(4)−S(8)	2.429(2)
Sb(3)−S(6)	2.4597(17)	Sb(4)−S(9)	2.4639(16)
Sb(3)−S(5)	2.598(2)	Sb(4)−S(10)	2.615(2)
Sb(3)−S(8)	3.120(3)	Sb(4)−S(7)	3.092(3)
Sb(3)−S(10)	3.359(3)	Sb(4)−S(5)	3.407(2)
Sb(5)−S(11)	2.4066(16)	Sb(6)−S(13)	2.4345(16)
Sb(5)−S(10)	2.538(3)	Sb(6)−S(14)	2.438(3)
Sb(5)−S(12)	2.662(2)	Sb(6)−S(12)	2.523(2)
Sb(5)−S(8)	3.012(3)	Sb(6)−S(8)	3.304(2)
Sb(5)−S(14)	3.138(3)	Sb(6)−S(10)	3.404(2)
Sr(1−-S(11)	3.003(2)	Sr(2)−S(4)	3.007(2)
Sr(1)−S(3)	3.006(2)	Sr(2)−S(3)	3.025(2)
Sr(1)−S(4)	3.050(2)	Sr(2)−S(13)	3.062(2)
Sr(1)−S(17)	3.063(2)	Sr(2)−S(11)	3.079(2)
Sr(1)−S(12)	3.099(3)	Sr(2)−S(14)	3.094(3)
Sr(1)−S(13)	3.104(2)	Sr(2)−S(15)	3.130(2)
Sr(1)−S(15)	3.143(2)	Sr(2)−S(17)	3.141(2)
Sr(1)−S(2)	3.183(3)	Sr(2)−S(1)	3.185(3)
Sr(1)−S(16)	3.260(2)	Sr(2)−S(16)	3.230(2)
Sr(3)−S(9)	3.001(2)	Sr(4)−S(14)	2.981(3)
Sr(3)−S(6)	3.002(2)	Sr(4)−S(6)	2.987(2)
Sr(3)−S(4)	3.019(2)	Sr(4)−S(3)	2.994(2)
Sr(3)−S(3)	3.023(2)	Sr(4)−S(9)	2.998(2)
Sr(3)−S(12)	3.069(3)	Sr(4)−S(4)	3.023(2)
Sr(3)−S(5)	3.084(3)	Sr(4)−S(7)	3.034(3)
Sr(3)-S(1)	3.110(3)	Sr(4)−S(2)	3.247(3)
Sr(5)−S(6)	3.016(2)	Sr(6)−S(13)	2.987(2)
Sr(5)−S(9)	3.024(2)	Sr(6)−S(9)	3.026(2)
Sr(5)−S(11)	3.032(2)	Sr(6)−S(6)	3.039(2)
Sr(5)−S(13)	3.064(2)	Sr(6)−S(8)	3.048(3)
Sr(5)−S(10)	3.093(3)	Sr(6)−S(11)	3.048(2)
Sr(5)−S(15)	3.100(2)	Sr(6)−S(17)	3.080(2)
Sr(5)−S(17)	3.136(2)	Sr(6)−S(15)	3.162(2)
Sr(5)−S(16)	3.200(2)	Sr(6)−S(16)	3.270(2)
Sr(5)−S(1)	3.456(3)	Sr(6)−S(2)	3.746(2)
S(15)−S(16)	2.090(3)	S(16)−S(17)	2.089(3)

around these sites. Unlike the Ba^{2+} ion, the Pb^{2+} ion possesses its $6s^2$ lone pair, which tends to distort more of the local environment. Therefore, the sulfur atoms need to adjust their positions slightly differently, depending on the identity of the metals in these disordered sites. The positional disorder for the S(1/1') and S(5/5') atoms is attributed to the same reason.

While $Ba_{2.62}Pb_{1.38}Sb_4S_{10}$ shares the same basic structural features with $Ba_3Sb_{4.66}S_{10}$, the atomic positions of the former deviate enough from those of the latter to destroy the *c*-glide plane perpendicular to the *b*-axis. As a result $Ba_{2.62}Pb_{1.38}Sb_4S_{10}$ lacks a center of inversion and adopts the polar space group $P2_1$. To visualize the difference in these two compounds, a center of inversion of the $Ba_3Sb_{4.66}S_{10}$ structure and the potential center of inversion of the $Ba_{2.62}Pb_{1.38}Sb_4S_{10}$ structure are x-marked in each unit cell; see Figures 3a and 5. A careful inspection of these figures reveals that most of the atoms in $Ba_{2.62}Pb_{1.38}Sb_4S_{10}$ and their "potential centrosymmetric pairs" are not well-related by the "center of inversion". Given that the polar members of the rathite group are strongly piezoelectric, it is anticipated that $Ba_{2.62}Pb_{1.38}Sb_4S_{10}$ will also be piezoelectric.

Relationship to Sulfosalt Minerals. These two compounds are closely related to the mineral lead sulfoarsenides, $(Pb,Tl)_3As_4(As,Ag)S_{10}$, $Pb_{3.5}As_{4.5}S_{10}$, $Pb_3As_5S_{10}$, and $Pb_4As_4S_{10}$, which are classified as the rathite group. These so-called rathite group compounds have the same basic framework as those of $Ba_3Sb_{4.66}S_{10}$ and $Ba_{2.62}Pb_{1.38}Sb_4S_{10}$ regardless of their compositional differences. However, as in the case of $Ba_3Sb_{4.66}S_{10}$ and $Ba_{2.62}Pb_{1.38}Sb_4S_{10}$, the atomic positions of each compound are altered enough to make each compound adopt different space groups. The cell parameters and the space groups for the minerals and the compounds reported here are shown in Table 8. All compounds possess 2_1 screw symmetry axes parallel to the *b*-axis. For clarification, however, we point out that the

Table 6. Selected Distances (Å) for $Ba_3Sb_{4.66}S_{10}$

Ba(1)−S(1)	3.0861(14)	Ba(2)−S(2)	3.2687(16)
Ba(1)−S(9)	3.1815(16)	Ba(2)−S(2)	3.2826(14)
Ba(1)−S(10	3.1832(17)	Ba(2)−S(3)	3.2869(14)
Ba(1)−S(7)	3.1857(15)	Ba(2)−S(7)	3.2877(17)
Ba(1)−S(9)	3.1902(15)	Ba(2)−S(4)	3.3161(14)
Ba(1)−S(6)	3.3059(15)	Ba(2)−S(3)	3.3366(15)
Ba(1)−S(8)	3.3442(15)	Ba(2)−S(4)	3.3375(16)
		Ba(2)−S(8)	3.3487(16)
Ba(3)−S(1)	3.1572(15)	Ba(2)−S(5)	3.4044(15)
Ba(3)−S(1)	3.2644(14)		
Ba(3)−S(8)	3.2821(17)		
Ba(3)−S(3)	3.3011(14)		
Ba(3)−S(7)	3.3096(16)	Sb(1)−S(1)	2.4078(14)
Ba(3)−S(3)	3.3461(15)	Sb(1)−S(3)	2.4115(14)
Ba(3)−S(4)	3.4103(14)	Sb(1)−S(2)	2.5027(14)
Ba(3)−S(4)	3.4349(15)	Sb(1)−S(6)	3.3349(15)
Ba(3)−S(6)	3.4776(15)	Sb(1)−S(5)	3.3809(16)
Sb(2)−S(4)	2.3861(13)	Sb(3)−S(7)	2.4223(14)
Sb(2)−S(5)	2.4920(14)	Sb(3)−S(6)	2.4386(14)
Sb(2)−S(2)	2.5671(14)	Sb(3)−S(5)	2.5039(15)
Sb(2)−S(6)	3.1107(16)	Sb(3)−S(9)	3.3294(17)
Sb(2)−S(1)	3.4167(15)	Sb(3)−S(10)	3.4459(17)
Sb(4)−S(8)	2.4179(14)	Sb(5)−S(10)	2.5645(19)
Sb(4)−S(9)	2.4652(15)	Sb(5)−S(10)	2.579(2)
Sb(4)−S(10)	2.6954(16)	Sb(5)−S(9)	2.7122(17)
Sb(4)−S(6)	2.9633(16)	Sb(5)−S(8)	2.9645(17)
		Sb(5)−S(7)	3.2175(19)
Sb(5)−S(9)	2.852(8)	Sb(5)−S(2)	3.409(2)
Sb(5)−S(2)	2.864(13)		
Sb(5)−S(10)	2.920(11)		
Sb(5)−S(7)	2.921(9)		
Sb(5)−S(8)	2.936(7)		
Sb(5)−S(10)	3.054(12)		
Sb(5)−Sb(5)	0.575(12)		

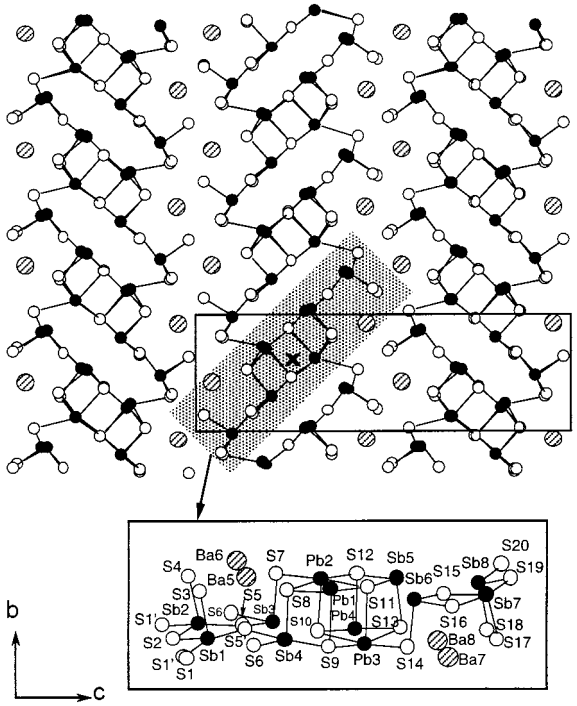

Figure 5. Structure of $Ba_{2.62}Pb_{1.38}Sb_4S_{10}$ viewed down the *a*-axis. The inset shows an asymmetric unit with the atomic labeling scheme.

Table 7. Selected Distances (Å) for $Ba_{2.62}Pb_{1.38}Sb_4S_{10}$

Pb(1)/Ba(1)−S(8)	2.848(7)	Pb(2)/Ba(2)−S(10)	2.681(9)
Pb(1)/Ba(1)−S(1)	2.86(3)	Pb(2)/Ba(2)−S(12)	2.811(6)
Pb(1)/Ba(1)−S(7)	2.869(8)	Pb(2)/Ba(2)−S(11)	2.820(6)
Pb(1)/Ba(1)−S(1)	2.91(3)	Pb(2)/Ba(2)−S(7)	3.048(7)
Pb(1)/Ba(1)−S(9)	2.989(9)	Pb(2)/Ba(2)−S(8)	3.084(7)
Pb(1)/Ba(1)−S(12)	3.350(6)	Pb(2)/Ba(2)-S(2)	3.298(8)
Pb(1)/Ba(1)−S(11)	3.365(6)		
Pb(3)/Ba(3)−S(11)	2.846(6)	Pb(4)/Ba(4)−S(12)	2.855(6)
Pb(3)/Ba(3)−S(14)	2.993(7)	Pb(4)/Ba(4)−S(14)	2.931(7)
Pb(3)/Ba(3)−S(13)	2.999(7)	Pb(4)/Ba(4)−S(13)	3.028(7)
Pb(3)/Ba(3)−S(10)	3.008(10)	Pb(4)/Ba(4)−S(20)	3.048(5)
Pb(3)/Ba(3)−S(19)	3.067(6)	Pb(4)/Ba(4)−S(10)	3.063(10)
Pb(3)/Ba(3)−S(9)	3.093(9)	Pb(4)/Ba(4)−S(9)	3.156(10)
Ba(5)−S(1)	3.16(3)	Ba(6)−S(2)	3.145(8)
Ba(5)−S(1)	3.23(3)	Ba(6)−S(2)	3.219(8)
Ba(5)−S(1)	3.23(3)	Ba(6)−S(4)	3.303(8)
Ba(5)−S(1)	3.24(3)	Ba(6)−S(3)	3.305(8)
Ba(5)−S(3)	3.262(8)	Ba(6)−S(3)	3.307(8)
Ba(5)−S(4)	3.276(8)	Ba(6)−S(4)	3.322(8)
Ba(5)−S(8)	3.294(7)	Ba(6)−S(7)	3.404(7)
Ba(5)−S(4)	3.337(8)	Ba(6)−S(5)	3.415(13)
Ba(5)−S(3)	3.342(8)	Ba(6)−S(8)	3.439(7)
Ba(5)−S(7)	3.344(8)	Ba(6)−S(5)	3.46(2)
Ba(5)−S(6)	3.527(8)		
Ba(7)−S(19)	3.217(6)	Ba(8)−S(20)	3.206(6)
Ba(7)−S(18)	3.265(6)	Ba(8)−S(18)	3.263(6)
Ba(7)−S(19)	3.275(6)	Ba(8)−S(20)	3.278(6)
Ba(7)−S(13)	3.286(7)	Ba(8)−S(18)	3.306(6)
Ba(7)−S(18)	3.317(6)	Ba(8)−S(17)	3.324(6)
Ba(7)−S(17)	3.326(6)	Ba(8)−S(13)	3.325(7)
Ba(7)−S(17)	3.365(6)	Ba(8)−S(14)	3.356(8)
Ba(7)−S(15)	3.401(6)	Ba(8)−S(17)	3.377(6)
Ba(7)−S(14)	3.403(7)	Ba(8)−S(16)	3.408(6)
Sb(1)−S(3)	2.429(8)	Sb(2)−S(4)	2.427(9)
Sb(1)−S(1)	2.53(3)	Sb(2)−S(1)	2.62(3)
Sb(1)−S(2)	2.540(8)	Sb(2)−S(2)	2.637(8)
Sb(1)−S(5)	2.63(2)	Sb(2)−S(5)	2.638(11)
Sb(1)−S(6)	3.089(10)	Sb(2)−S(6)	3.074(10)
Sb(1)−S(1)	3.09(3)	Sb(2)−S(1)	3.15(3)
Sb(1)−S(5)	3.214(12)	Sb(2)−S(5)	3.233(17)
Sb(3)−S(7)	2.498(9)	Sb(4)−S(8)	2.502(8)
Sb(3)−S(5)	2.661(12)	Sb(4)−S(5)	2.637(17)
Sb(3)−S(6)	2.710(10)	Sb(4)−S(6)	2.750(10)
Sb(3)−S(9)	2.871(9)	Sb(4)−S(9)	2.795(10)
Sb(3)−S(10)	3.106(10)	Sb(4)−S(10)	3.038(10)
Sb(3)−S(5)	3.32(2)	Sb(4)−S(5)	3.305(11)
Sb(5)−S(13)	2.504(7)	Sb(6)−S(15)	2.443(5)
Sb(5)−S(12)	2.572(6)	Sb(6)−S(16)	2.446(5)
Sb(5)−S(11)	2.586(6)	Sb(6)−S(14)	2.449(7)
Sb(5)−S(16)	3.294(5)	Sb(6)−S(11)	3.278(6)
Sb(5)−S(15)	3.347(6)	Sb(6)−S(12)	3.289(6)
Sb(7)−S(17)	2.370(6)	Sb(8)−S(18)	2.414(6)
Sb(7)−S(15)	2.615(6)	Sb(8)−S(20)	2.415(5)
Sb(7)−S(16)	2.686(5)	Sb(8)−S(19)	2.431(5)
Sb(7)−S(19)	2.949(6)	Sb(8)−S(16)	3.348(5)
Sb(7)−S(20)	3.043(5)	Sb(8)−S(15)	3.369(5)
S(1)−S(1)	0.67(3)	S(5)−S(5)	0.833(19)

b-axes of dufrenoysite and rathite-Ia are differently chosen from the rest of the compounds, so the screw axes in these compounds lie in different directions. It is also worthwhile to notice that rathite-I, $Ba_3Sb_{4.66}S_{10}$, and $Ba_{2.62}Pb_{1.38}Sb_4S_{10}$ have β angles of ~100°, while the others have β angles of ~90°. It is not due to any significant structural distortions but arises because one of the cell axes is chosen differently in such a way that the resulting cell volume is $\sqrt{2}$ times larger than those of the compounds with the β of ~90°. Therefore, strictly speaking these compounds are not isostructural with one another. Only dufrenoysite and rathite-Ia are isostructural and so are $Ba_3Sb_{4.66}S_{10}$ and rathite-I with the a- and *c*-axes switched.

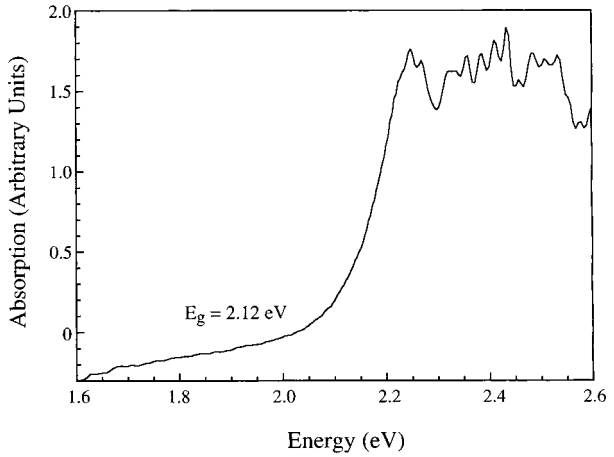

Figure 6. Optical absorption spectrum of $Sr_6Sb_6S_{17}$. The band gap value, E_g, is shown in the figure.

Another main difference among these compounds lies in the divalent (Pb^{2+}) to trivalent (As^{3+}) ion ratio. As mentioned previously $Pb_4As_4S_{10}$ is the only compound that satisfies charge neutrality with a divalent to trivalent metal ratio equal to 1. Therefore, other compounds, which possess a ratio smaller than 1, are suspected to have partial occupancy in certain As sites as the Sb(5/5') site of $Ba_3Sb_{4.66}S_{10}$. It is mostly the (6 + 1) sites with disorder between As and Pb, whereas the nine-coordinate sites are fully occupied with Pb atoms and the three-coordinate sites are filled with As ions. It seems that this structure type can tolerate considerable compositional variety without disrupting the basic framework. This is possible by allowing mixed occupancy between trivalent and divalent ions or partial occupancy of the trivalent ion in the highly flexible (6 + 1) sites. On the basis of these observations, a relatively large number of interesting derivatives may be expected here, many of them with interesting piezoelectric and nonlinear optical (NLO) properties.

3.2. Spectroscopic Characterization and Thermal Analysis. The materials described here are valence-precise and are expected to be semiconductors. The optical absorption spectrum of $Sr_6Sb_6S_{17}$ is shown in Figure 6. The compound shows an abrupt optical gap at 2.10 eV consistent with its red color. $Ba_3Sb_{4.66}S_{10}$ and $Ba_{2.62}Pb_{1.38}Sb_4S_{10}$ also exhibit clean optical band gaps at 2.14 and 1.64 eV, respectively. The introduction of heavy Pb atom in the structure dramatically decreases the band gap by 0.5 eV; see Figure 7. This is attributed to the more covalent and less ionic Pb−S bonding compared to Ba−S bonding. The polar structure of $Ba_{2.62}Pb_{1.38}Sb_4S_{10}$ may make it an interesting material for NLO investigations. The spectrum of $Ba_{2.62}Pb_{1.38}Sb_4S_{10}$ shows very little light absorption below the band gap transition, which bodes well for NLO experiments.

Table 8. Crystallographic Data for $Ba_3Sb_{4.66}S_{10}$, $Ba_{2.62}Pb_{1.38}Sb_4S_{10}$, and the Related Sulfosalt Minerals

formula	mineral	*a* (Å)	*b* (Å)	c (Å)	β (deg)	SG
$Pb_4As_4S_{10}$	dufrenoysite	7.90	25.74	8.37	90.21	$P2_1$
$Pb_{3.5}As_{4.5}S_{10}$	rathite-Ia	7.91	25.80	8.43	90	$P2_1$
$(Pb,Tl)_3As_4(As,Ag)S_{10}$	rathite-I	25.16	7.94	8.47	100.28	$P2_1/a$
$Pb_3As_5S_{10}$	rathite-III	24.52	7.91	8.43	90	$P2_1$
$Ba_3Sb_{4.66}S_{10}$		8.955	8.225	26.756	100.29	$P2_1/c$
$Ba_{2.62}Pb_{1.38}Sb_4S_{10}$		8.8402	8.2038	26.7623	99.488	$P2_1$

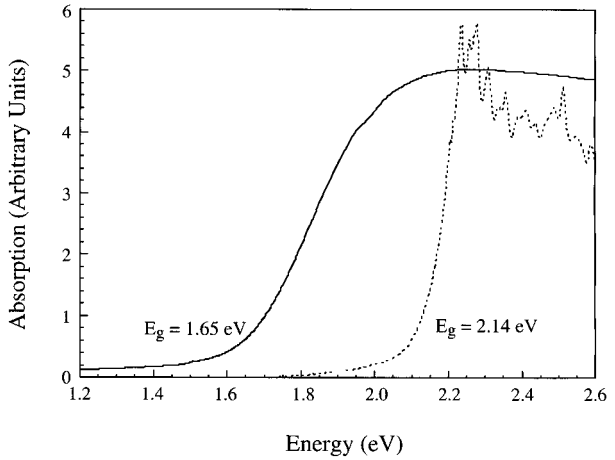

Figure 7. Optical absorption spectra of $Ba_3Sb_{4.66}S_{10}$ (—) and $Ba_{2.62}Pb_{1.38}Sb_4S_{10}$(···). The band gap values, E_g, are shown.

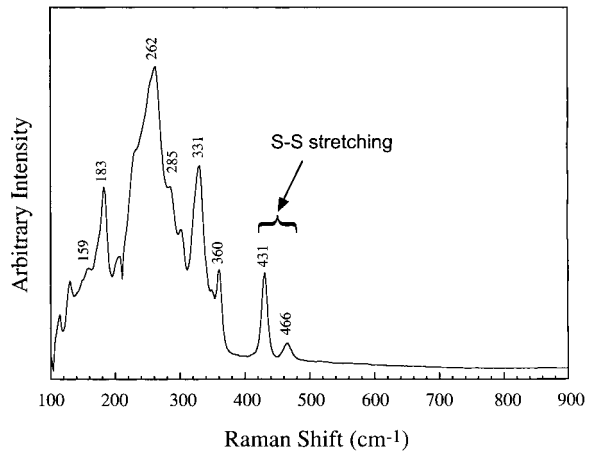

Figure 8. Raman spectrum of $Sr_6Sb_6S_{17}$.

The Raman spectrum of $Sr_6Sb_6S_{17}$ is shown in Figure 8. The shift at 431 and 466 cm^{-1} are assigned to the symmetric and antisymmetric S−S stretching vibrations of trisulfide groups. These values are in accord with the corresponding frequencies reported for other compounds with the trisulfide groups such as $\nu_s(SS) = 441$ cm^{-1} and $\nu_a(SS) = 476$ cm^{-1} for K_2S_3.[22] The Raman spectra of $Ba_3Sb_{4.66}S_{10}$ and $Ba_{2.62}Pb_{1.38}Sb_4S_{10}$ are shown in Figure 9. They share similar features with that of $Sr_6Sb_6S_{17}$, only this time the S−S stretching modes are absent. The highest energy shifts appear at 360 cm^{-1} for $Ba_3Sb_{4.66}S_{10}$ and 348 cm^{-1} for $Ba_{2.62}Pb_{1.38}Sb_4S_{10}$, both of which are generated by Sb−S vibrations. The reason for the lower energy shift of Sb−S stretching in $Ba_{2.62}Pb_{1.38}Sb_4S_{10}$ is attributed to the participation of the heavier Pb atoms bonded to the thioantimonate framework.

Differential thermal analysis (DTA) suggests that these compounds melt congruently at 729, 770, and 749 °C for $Sr_6Sb_6S_{17}$, $Ba_3Sb_{4.66}S_{10}$, and $Ba_{2.62}Pb_{1.38}Sb_4S_{10}$, respectively. For each compound, multiple heating/cooling cycles were monitored, as shown in Figure 10 for $Ba_{2.62}Pb_{1.38}Sb_4S_{10}$, which exhibits well-defined melting and crystallization points. The powder XRD patterns, which were taken before and after DTA measurement, are identical, indicating no decomposition.

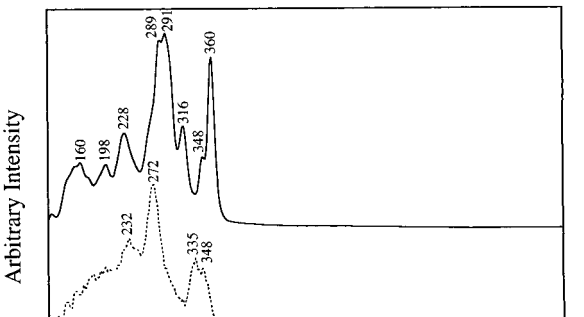

Figure 9. Raman spectra of $Ba_3Sb_{4.66}S_{10}$ (—) and $Ba_{2.62}Pb_{1.38}Sb_4S_{10}$-(···).

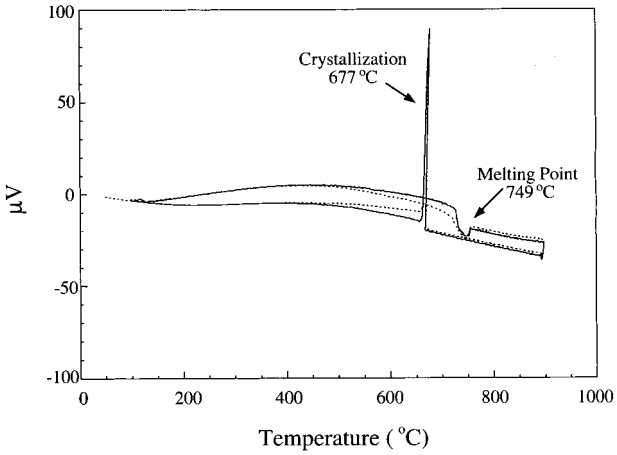

Figure 10. DTA diagram of $Ba_{2.62}Pb_{1.38}Sb_4S_{10}$: (—) first cycle; (···) second cycle.

Acknowledgment. Financial support from the National Science Foundation (Grant DMR-9817287) is gratefully acknowledged. This work made use of the W. M. Keck Microfabrication facility at MSU, a NSF MRSEC facility. This work made use of the SEM facilities of the Center for Electron Optics at Michigan State University.

Supporting Information Available: Tables of crystallographic details, atomic coordinates, isotropic and anisotropic displacement parameters for all atoms, and interatomic distances and angles for the substructure and the superstructure of $Sr_6Sb_6S_{17}$, $Ba_{2.62}Pb_{1.38}Sb_4S_{10}$, and $Ba_3Sb_{4.66}S_{10}$. This material is available free of charge via the Internet at http://pubs.acs.org.

IC000632M

(22) Jaroudi, O. E.; Picquenard, E.; Demortier, A.; Lelieur, J.-P.; Corset, J. *Inorg. Chem.* **1999**, *38*, 2394−2401.